The Motion of Taylor Bubbles in Vertical Tubes.
I. A Numerical Simulation for the Shape
and Rise Velocity of Taylor Bubbles in
Stagnant and Flowing Liquid

ZAI-SHA MAO* AND A. E. DUKLER

*University of Houston, Department of Chemical Engineering,
Houston, Texas 77204-4792*

A numerical method has been developed for computing the velocity field adjacent to a free surface along with the surface shape for situations where both the inertial and viscous terms are important. The method is used to predict the shape and rise velocity of a Taylor bubble in stagnant or flowing liquid. Multiple theoretical solutions are shown to exist and the criterion for selecting the physically observable solution is indicated.   © 1990 Academic Press, Inc.

1. INTRODUCTION

When gas and liquid flow simultaneously upward in vertical tubes, the two phases distribute in a pattern known as slug flow for a wide range of flow rate pairs. This pattern occurs in a variety of industrial situations including geothermal, oil, and gas wells, oil–gas pipelines, steam generating boilers, and during emergency core cooling of a nuclear reactor among many such examples. Slug flow (Fig. 1) is characterized by the pseudo-periodic occurrence of large bullet-shaped bubbles which have a round nose, a comparatively flat bottom and occupy most of the cross-sectional area (referred to as a Taylor bubble). The liquid moves upwards as an aerated slug (referred to as a liquid slug) between two successive Taylor bubbles and flows downwards in the form of a liquid film around the Taylor bubble. Taylor bubbles and liquid slugs are alternatively spaced in the tube. Fernandes *et al.* [1] developed a detailed model for this type of flow which demonstrated that the flow characteristics of such systems (pressure pulsations, slug, and bubble lengths, holdup, pressure losses etc.) depend critically on the rise velocity of the Taylor bubbles. In order to advance the understanding of this complex system, we develop a numerical method for finding the bubble shape and translation velocity and examine solutions for single Taylor bubbles travelling in unaerated liquid, either at rest or moving upward at a prescribed velocity. While the methodology is

---

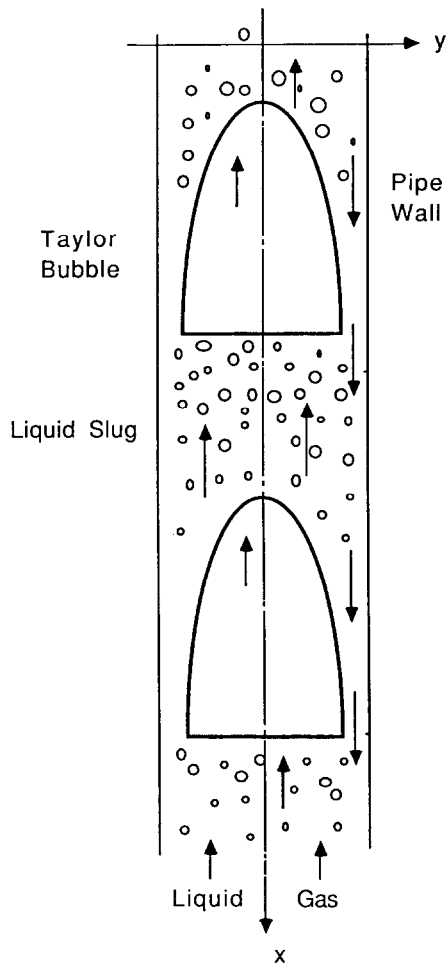* Present address: Institute of Chemical Metallurgy, Academia Sinica, Beijing, China.

FIG. 1. Sketch of continuous slug flow.

developed in the context of this particular application we suggest that it is more generally applicable to the class of problems where both inertial and viscous forces must be considered and where free surfaces exist.

Theoretical and experimental attention to this problem of the rise velocity of a Taylor bubble has been ongoing for almost a half century. A major line of attack for a Taylor bubble in a tube was initiated by Dumitrescu [2], who considered the problem as one of potential flow around an axisymmetric Taylor bubble with viscous effects neglected. This was followed over the years by theoretical contributions of Davis and Taylor [3], Collins [4], Collins *et al.* [5], and most recently Bendiksen [6] and Nickens and Yannitell [7]. All of these investigators took the

fluid as inviscid. But in the film receding from the nose, viscous effects are impor-
tant. Brown [8] tried to match the solution for potential flow with that for the thin
receding viscous film with only partial success. The same potential flow approach
was used for plane Taylor bubbles rising between parallel plates by Birkhoff and
Carter [9], Garabedian [10], Vanden-Broeck [11], and Couöt and Strumulo [12].
In contrast, a series of attacks on the problem wherein the inertial terms were
neglected, the creeping flow approximation adopted and thus the process con-
sidered as viscosity dominated appear to have been initiated by Bretherton [13]
and followed, among others, by Goldsmith and Mason [14], Friz [15], and more
recently by Reinelt [16]. Despite the linearity of the Navier–Stokes equations as a
result of the creeping flow assumption, analytical solutions were possible only using
additional assumptions and simplifications. It was only in 1987 that a full numerical
solution of the creeping flow problem was generated and this was expensive in
computer time [16]. To the knowledge of the authors, no general solution of
the problem has appeared in which both the convective and viscous terms of the
equations of motion are retained.

Many experimental investigations on this subject have also been conducted.
Harmathy [17] and White and Beardmore [18] did systematic experimental
measurements of the rise velocity of axisymmetric bubbles in vertical tubes, Zukoski
[19] and Weber *et al.* [20] explored the effect of tube inclination on the translation
velocity. Corresponding studies for the plane bubble were reported by Maneri and
Zuber [21].

In this paper, a method is developed for solving the flow field around a Taylor
bubble. The problem is particularly challenging because the shape of the interface
between gas and liquid cannot be specified in advance and determining this shape
and thus determining the computational domain is, itself, part of the problem. For
the purpose of clarity, only the case of laminar flow is addressed in this paper. With
the structure of the algorithm established, the method can readily be extended to
include a turbulence model for higher flow rates and this is done in a followup
paper by Mao and Dukler [22], where comparison with experimental data is
included.

2. FORMULATION OF THE PROBLEM AND THE SOLUTION STRATEGY

Consider a single Taylor bubble of finite length moving at a velocity U_N relative
to the fixed walls in a liquid which is also flowing upward (Fig. 2a). This unsteady
problem becomes a steady one if the reference frame moves at the velocity of the
Taylor bubble U_N (Fig. 2b). The transformation of coordinates system is simply

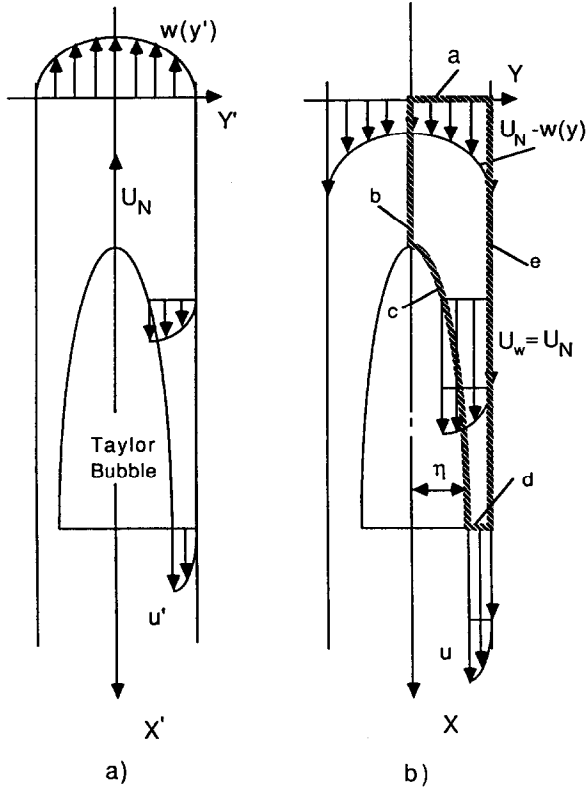$$x = x' - U_N t,$$

$$y = y',$$

Fig. 2. A Taylor bubble rising in a vertical pipe: (a) in fixed coordinates; (b) in moving coordinates.

which fixes the Taylor bubble relative to the coordinate system. If a new velocity variable, u, is defined as

$$u = u' + U_N,$$

the Navier–Stokes equation becomes a steady-state one,

$$\rho \mathbf{u} \cdot \nabla \mathbf{u} = -\nabla p + \mu \nabla^2 \mathbf{u},$$

to be solved together with the continuity equation,

$$\nabla \mathbf{u} = 0,$$

subject to a set of boundary conditions. In a two-dimensional coordinate system, the equations are

$$\frac{\partial}{\partial x}(\rho u u)+\frac{1}{r}\frac{\partial}{\partial y}(\rho v u)=-\frac{\partial p}{\partial x}+\frac{\partial}{\partial x}\left(\mu\frac{\partial u}{\partial x}\right)+\frac{1}{r}\frac{\partial}{\partial y}\left(r\mu\frac{\partial u}{\partial y}\right),\tag{1}$$

$$\frac{\partial}{\partial x}(\rho u v)+\frac{1}{r}\frac{\partial}{\partial y}(r\rho v v)=-\frac{\partial p}{\partial y}+\frac{\partial}{\partial x}\left(\mu\frac{\partial v}{\partial x}\right)+\frac{1}{r}\frac{\partial}{\partial y}\left(r\mu\frac{\partial v}{\partial y}\right)-\left\{\mu\frac{v}{r^2}\right\},\tag{2}$$

$$\frac{\partial}{\partial x}\rho u+\frac{1}{r}\frac{\partial}{\partial y}(r\rho v)=0,\tag{3}$$

following the form given by Pope and Whitelaw [23], where $r \equiv 1$ for Cartesian coordinates, $r \equiv y$ for cylindrical coordinates and curly brackets indicate the terms present only in cylindrical coordinates.

The domain of solution consists of the axisymmetric volume enclosed by surfaces a–b–c–d–e shown in Fig. 2b. A no slip boundary condition exists at the wall (along e). Experimental data show that the entire Taylor bubble is a region of constant pressure. The curved interface of the Taylor bubble (along c) is thus a free surface along which the shear stress is uniformly zero and the following conditions exist:

$$(\bar{\tau}\cdot\mathbf{n})\cdot\mathbf{s}=0,\qquad\text{(zero interfacial shear stress)}\tag{4}$$

$$\mathbf{u}\cdot\mathbf{n}=0,\qquad\text{(kinematic condition)}\tag{5}$$

$$p_{iL}+\sigma K=\text{const.}\qquad\text{(normal stress balance)}.\tag{6}$$

Scaling arguments can be used to show that the viscous terms can be neglected in Eq. (6) for nominal viscosities. The curvature K is defined as

$$K=\frac{1}{r_1}+\frac{1}{r_2},\tag{7}$$

σ is the surface tension, and r_1, r_2 the local principal radii of curvature at the bubble surface,

$$r_1=\sqrt{\left(1+\left(\frac{d\eta}{dx}\right)^2\right)^3}\Big/-\frac{d^2\eta}{dx^2},\tag{8a}$$

$$r_2=n\sqrt{1+\left(\frac{d\eta}{dx}\right)^2},\tag{8b}$$

p_{iL} is the pressure on the liquid side of the interface (the viscous normal stress included), and $\eta(x)$ the radial distance from the axis to the interface describing the shape of the bubble; $\bar{\tau}$ is the shear tensor, $\mathbf{n}$ the unit normal vector, and $\mathbf{s}$ the unit tangential vector at the interface. The shape of the curve is unknown in advance of the numerical simulation, hence it is part of the solution. The downstream boundary conditions (along d) are chosen such that the flow is parallel and the velocity gradient is zero in the x direction. Upstream (along a) the liquid flows with

a fully developed velocity distribution $w(y')$ in fixed coordinates, and $U_N - w(y)$ in moving coordinates.

The problem can be summarized as follows: with known diameter of tube, length of the Taylor bubble and physical properties of the fluid, determine the shape of the Taylor bubble, its translation velocity, and the velocity at all positions in the liquid around the bubble. The mathematical task can be similarly set for slightly modified boundary conditions. The case of two Taylor bubbles in a continuous slug flow will be addressed in a sequel of this paper.

The strategy of solution is to subdivide the problem into three steps:

(1) Solve for the flow field around a Taylor bubble subject to appropriate boundary conditions, but with an initially assumed shape and U_N;

(2) Adjust the shape function $\eta(x)$ in a prescribed fashion to satisfy the balance of normal stress at the interface such that constant pressure is maintained in the bubble and no flow takes place across its interface.

(3) Adjust U_N to satisfy the criterion that a symmetric Taylor bubble is locally spherical at the nose in the presence of nonzero interfacial tension

These three steps are detailed in Sections 3 through 5. The computational scheme involves (a) the construction of a special grid system particularly suited to accurately applying the boundary conditions at the interface, (b) the use of differencing method developed here for handling the strong convection terms in problems of this type where the grid spacing is highly nonuniform and when the velocity can be strongly skewed to the coordinates of the grid, (c) modifying the shape by the use of a corrector differential equation, (d) incorporating the effect of the surface tension which introduces third order into the problem through a first-order effect differential equation approximation, and (e) adjusting the rise velocity according to the value of the gradient of the curvature at the nose.

3. COMPUTATIONAL SCHEME GIVEN A SHAPE PROFILE AND A RISE VELOCITY

The numerical method selected is the control volume approach outlined in detail by Patankar [24]. This method incorporates some of the characteristics of finite-difference as well as finite-element methods. The momentum equations are integrated over a control volume consisting of a single specific cell as done in finite-element methods. This yields a discretized equation which involves the parameters of the adjacent cells as in finite-difference methods. A staggered pattern of allocation of velocity components u, v, and the pressure p nodes is used as shown in Fig. 3 for typical interior and surface locations. The nodes for pressure are also the location of other scalar parameters such as temperature or concentration when appropriate with u and v nodes located on the faces of a p cell.
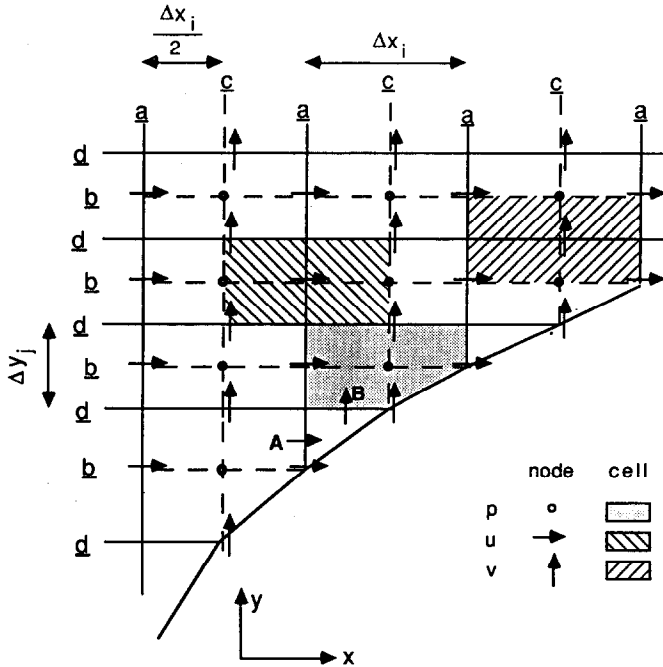
FIG. 3. A staggered distribution of nodes in the interior and on the boundary. An incomplete pressure cell is shown at the border curve.

The Gridding System

In order to satisfy the condition of zero stress along the free surface, high enough accuracy is needed to compute reliable values of the derivatives of the velocity components. For this purpose a gridding scheme of the type suggested by Williamson [25] is applied to this problem but with velocity and pressure cells generated by the grid assigned in a particular way such that the interfacial shear stress condition can be applied accurately. This special gridding procedure is illustrated in Fig. 3.

Lines of constant x are drawn through the interface with spacing Δx_i selected to be smaller in regions of larger curvature of the surface. These lines are marked (a) in Fig. 3. Nodes for the surface u cells are designated where these lines intersect the surface. Constant y grid lines, marked (b), are then drawn to intersect with these u nodes on the surface. The spacing Δy_j is thus determined by the curvature of the surface and varies with position. The (a) and (b) lines drawn in this way create the v cells. v and p nodes are located as follows: Dashed vertical lines marked (c) are located midway between each adjacent pair of constant x lines. Where this intersects the interface is the surface v node. Horizontal lines marked (d) are extended from the surface v nodes. Each intersection of an (a) and (b) line is a u node, the intersection of (c) and (d) lines is a v node and the intersection of (b) and (c) lines

a p node. In this way the staggered network of nodes and their cells are formed. All interior u and v cells over which the balances of momentum are made are rectangular. Variables u and v at the surface are obtained by applying the surface boundary conditions as described below. Values of p on the surface are obtained by nonlinear extrapolation from the interior nodes. Now all the interpolation and extrapolation are performed with the same scheme because all the incomplete cells are topologically the same. The disadvantage of this grid system rests in its non-uniformity of gridline spacing, which is less accurate for a fixed number of grid lines than is a uniform distribution. Desired accuracy can be achieved by using more grid lines or a better differencing scheme. However, no partial velocity cells exist at the interface; thus the boundary conditions which exist there can be satisfied accurately.

When the p cells are formed, certain uncovered spaces exist near the interface as shown in Fig. 3. The p cells are used only to execute a material balance using the SIMPLE algorithm [24] in order to test and adjust the pressure field. This balance can be accurately accomplished in these partial cells by equating the flow indicated by arrow A to that by arrow B. In this way a surface-fitted staggered coordinate system has been created which is particularly suitable for applying a surface stress condition.

The gas–liquid interface is regarded as a free surface without shear stress and at constant pressure. In Cartesian coordinates and for a Newtonian fluid, the interfacial shear stress condition Eq. (4) reads

$$\tau_i = \mu \left[2n_x n_y \left(\frac{\partial v}{\partial y} - \frac{\partial u}{\partial x} \right) + (n_x^2 - n_y^2) \left(\frac{\partial u}{\partial y} + \frac{\partial v}{\partial x} \right) \right], \tag{9}$$

where μ is the liquid viscosity, n_x and n_y are the x and y components of the unit normal to the surface, and subscript i stands for the interface. Given a surface shape, the surface velocities are obtained by application of Eq. (9) with the prescribed surface shear stress τ_i and the kinematic condition at the interface, Eq. (5), which now reads

$$n_x u_i + n_y v_i = 0. \tag{10}$$

The procedure can be understood by reference to Fig. 4 for the case where $\tau_i = 0$. At each iteration the interior of the domain is solved first. Then v_2, v_3, v_4, and v_5 are obtained by interpolation from values at the adjacent nodes. Quadratic interpolation formulas are then employed for the gradient terms in Eq. (9) using u_1, u_2, and u_3 for $\partial u / \partial x$; u_1, u_4, and u_5 for $\partial u / \partial y$; v_1, v_2, and v_3 for $\partial v / \partial x$; v_1, v_4, and v_5 for $\partial v / \partial y$. Since all the interior velocities are available from the interior nodes, the only unknowns in Eq. (9) are the surface velocities, u_1 and v_1. These two quantities can thus be determined between Eqs. (9) and (10). The velocity at the v_i node located on the surface between two u_i nodes is obtained by interpolation.

Differencing Process

The differential equation to be solved is first integrated over the control volume of a cell in the sense that the fluxes at all faces of a cell are in balance with the
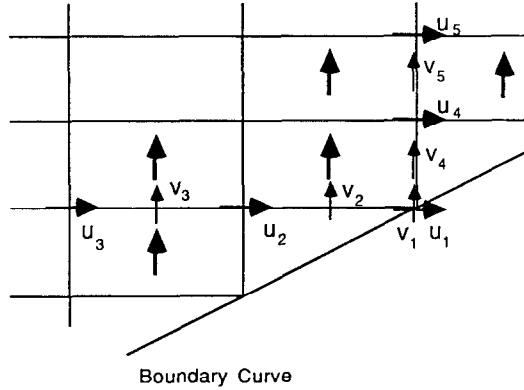
Boundary Curve

FIG. 4. Evaluation of the velocity gradients needed for the shear stress condition at the surface.

accumulation and source terms inside the cell. Then the process of discretization is carried out. The flux J on each face of a cell is determined from the values at the neighboring nodes and the properties on the faces. The final form of the discretized momentum equation will depend upon the differencing scheme used to estimate the fluxes across the faces of a cell due to convection and diffusion. A large variety of differencing schemes have been proposed in the past, among which are central difference scheme (CDS), upstream hybrid difference scheme (UHDS), upstream power-law difference scheme (UPDS), skew upstream difference scheme (SUDS), and skew upstream weighted difference scheme (SUWDS).

The balance of the transport fluxes through all the cell faces, J, and source terms, S'_ϕ, over a cell for a transportable physical variable, ϕ, is

$$J_e - J_w + J_n - J_s = S'_\phi, \tag{11}$$

which results in a steady-state two-dimensional discretized differential equation,

$$a_P \phi_P = \sum_{nb} a_{nb} \phi_{nb} + S_\phi, \tag{12}$$

where the coefficient a for the center node is

$$a_P = \sum_{nb} a_{nb},$$

and S_ϕ is nominally the source term, subscripts n, e, s, and w denote the four faces of the cell, p for the center node, nb representing the north, east, south and west neighboring nodes. In order to guarantee the convergence in solving iteratively the resulting algebraic equation set, all those differencing schemes manage to make the a_{nb}'s positive. If care is taken in expressing S_ϕ in terms of ϕ_P, the convergence of

solution of Eq. (12) is assured. The boundary conditions can be easily incorporated by means of pseudo-source terms as explained by Patankar [24].

Early versions of these ideas were implemented with UHDS by Gosman *et al.* [26] in a computer code designated as TEACH and successfully used to solve a variety of problems in single phase flow and transport of scalar quantities (for example, Armaly and Durst [27]). This program was shown to be efficient and stable for high Reynolds number flows. However, Leonard [28] and Leschnizer and Rodi [29] documented the fact that UHDS is subject to significant errors due to numerical diffusion as a result of truncation in interpolation and evaluation of convection terms. The damage from this procedure is shown to be especially severe when the flow is highly skewed relative to the numerical mesh and the streamwise grid Peclet number, $P = V\Delta/v$, exceeds 2, where V is the absolute value of characteristic fluid velocity in the concerned direction of coordinate axis, Δ the mesh size in the same direction, and v the kinematic diffusivity for the transported variable. This situation exists in the case of a rising Taylor bubble especially at the highly curved interface near the nose region of the bubble. Thus it became necessary to explore alternative differencing schemes.

Studies by Leonard [28], Pollard and Siu [30], and Huang *et al.* [31] compare various schemes. From their work it is apparent that when using quadratic interpolation the difference equations become accurate to terms including the second derivative and numerical diffusion is sharply decreased. The advantages of this method of Leonard [28], called *quadratic upstream interpolation for convective kinematics* (QUICK), are particularly important when convection terms are dominant as they are here and when the spacing between the grids changes rapidly as is the case near the nose of the bubble. A revised version of this differencing scheme was developed for control volume formulation by Pollard and Siu [30] and is designated QUICKER. In applying this scheme to control volume formulation a nine-point configuration in Fig. 5 is used. ϕ at west and east faces, ϕ_w and ϕ_e, can be interpolated quadratically in one of the following two ways depending upon the sign of u_w and u_e:

$$\phi_w = \alpha_w \phi_{WW} + \beta_w \phi_W + \gamma_w \phi_P, \qquad \text{if} \quad u_w > 0, \tag{13a}$$

$$\phi_w = \delta_w \phi_E + \varepsilon_w \phi_P + \zeta_w \phi_W, \qquad \text{if} \quad u_w < 0, \tag{13b}$$

$$\phi_e = \alpha_e \phi_W + \beta_e \phi_P + \gamma_e \phi_E, \qquad \text{if} \quad u_e > 0, \tag{14a}$$

$$\phi_e = \delta_e \phi_{EE} + \varepsilon_e \phi_E + \zeta_e \phi_P, \qquad \text{if} \quad u_e < 0, \tag{14b}$$

where the interpolation coefficients are relied on the grid system. Similar expressions can be written for interpolation of ϕ_s and ϕ_n. In order to ensure all the coefficients in Eq. (12) positive, Pollard and Siu [30] manipulated the choice of a_{nb} such that they are always positive and absorbed the remaining terms into a source term. Wasden [32] extended the QUICKER to non-uniform grids. In order to promote convergence, the algorithm is further modified in this work to make use of the upstream-dominant nature of flow of low viscosity fluid. The coefficients a_{nb}
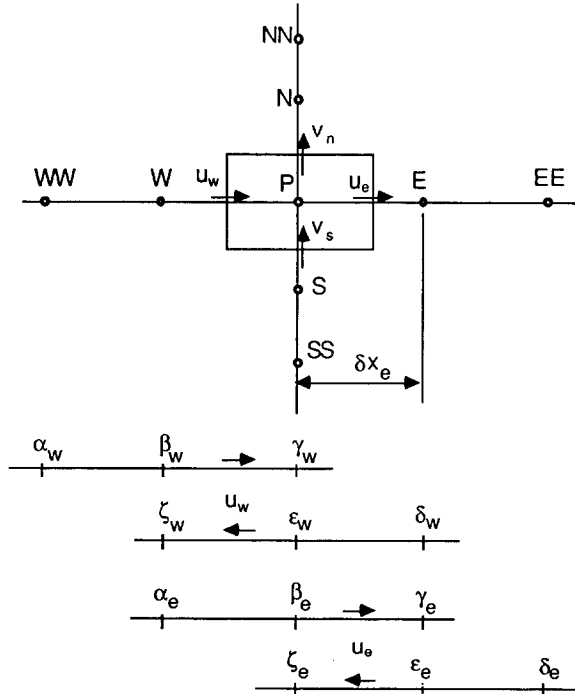
FIG. 5. A nine-point configuration for discretization by the QUICK algorithm at node P. The interpolation coefficients used to obtain values of the parameter at west and east faces are denoted; two upstream nodes are always used in the interpolation.

for the downstream interfaces are manipulated such that they simply consist of the part due to diffusion,

$$D_i = \frac{\mu}{(\delta x)_i}, \qquad i = n, e, s, \text{ or } w,$$

where $(\delta x)_i$ is the distance between the center node and a neighboring node. Thus a_{nb} is smaller in magnitude compared with the upstream ones. Numerically, the downstream flow has a weaker influence on the process of solution in the current iteration. Specified upstream boundary conditions thus convey their influence more quickly to the flow field. Meanwhile any possible numerical disturbance is more difficult to propagate upstream and cause divergence. After this modification, the coefficients read

$$a_e = \ddagger D_e, (D_e - \varepsilon_e C_e)^0, \tag{15a}$$

$$a_w = \ddagger D_w, (D_w + \beta_w C_w)^0, \tag{15b}$$

$$a_n = \ddagger D_n, (D_n - \varepsilon_n C_n)^0, \tag{15c}$$

$$a_s = \ddagger D_s, (D_s + \beta_s C_s)^0, \tag{15d}$$

where C_i is the mass flux through the cell faces. If the flow is from the east to the west, both C_e and C_w are negative and we will have $a_e = D_e - \varepsilon_e C_e$, which is greater than $a_w = D_w$. The source terms become more complex,

$$S_a = \alpha_w M_w^+ C_w \phi_{WW} + \alpha_s M_s^+ C_s \phi_{SS} - \delta_e M_e^- C_e \phi_{EE} - \delta_n M_n^- C_n \phi_{NN}$$
$$- M_e^+ C_e (\alpha_e \phi_W + \gamma_e \phi_E) - M_n^+ C_n (\alpha_n \phi_W + \gamma_n \phi_N)$$
$$+ M_w^- C_w (\delta_w \phi_E + \zeta_w \phi_W) + M_s^- C_s (\delta_s \phi_N + \zeta_s \phi_S), \tag{16}$$

$$S_b = -\beta_e M_e^+ C_e - \beta_n M_n^+ C_n + \varepsilon_w M_w^- C_w + \varepsilon_s M_s^- C_s$$
$$+ (\beta_s + \gamma_s) M_s^+ C_s + (\beta_s + \gamma_s) M_w^+ C_w$$
$$- (\varepsilon_e + \zeta_e) M_e^- C_e - (\varepsilon_n + \zeta_n) M_n^- C_n, \tag{17}$$

where

$$M_i^+ = \frac{C_i + |C_i|}{2C_i}, \qquad M_i^- = \frac{C_i - |C_i|}{2C_i}, \qquad i = n, e, s, w. \tag{18}$$

The modified program converges with a relaxation factor of 0.5 and the speed of convergence is satisfactory. As an illustration of the suitability of the revised QUICKER algorithm vs UPDS, calculations were made of the pressure profile along the prescribed free surface of a Taylor bubble using both methods. The results in Fig. 6 show that computational results are essentially independent of grid size using the revised QUICKER algorithm in contrast to results from UPDS.

In order to solve for the pressure field, the continuity equation is used in an algorithm designated SIMPLE (semi-implicit method for pressure-linked equations) by Patankar and Spalding [33]. The pressure does not appear explicitly in the continuity equation, but given a pressure field the velocity distributions can be obtained numerically from the momentum equations. Then a test is made to see if the continuity equation is satisfied. SIMPLE incorporates a procedure to solve for the correction needed to the pressure as well as the velocity fields u and v to minimize the discrepancy before the next iteration is invoked. Relaxation is necessary when applying the corrections to existing pressure and velocity fields. The correction on the u and v fields may lead to deviation from the momentum balance, therefore an iterative loop is designed; the solution proceeds in a loop structure for u, v, and p in sequence, followed by other scalar parameters such as temperature or turbulence parameters, where applicable. All the discretized algebraic equation sets are solved by the alternating direction implicit (ADI) method with suitable relaxation.

The Computed Results

Thus, given the domain including the shape of the free surface, the translation velocity of the bubble, an initial distribution of velocities, pressure, and the shear stress distribution along the interface, the code converges to specific velocity and pressure fields. Figure 7 shows the stream function contour map for a bubble rising
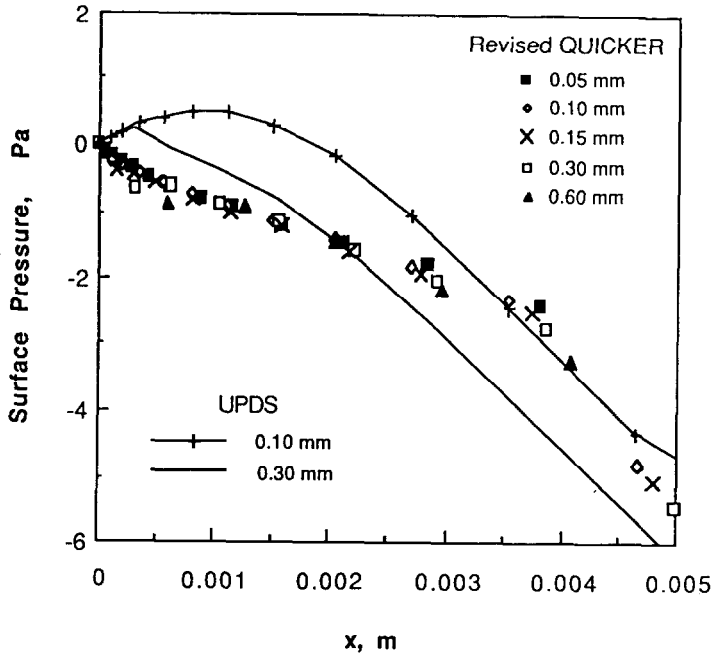
FIG. 6. Sensitivity to grid size of computed pressure at the free surface for UPDS and the revised QUICKER algorithms. The size of the nose cell is annotated in the legend.
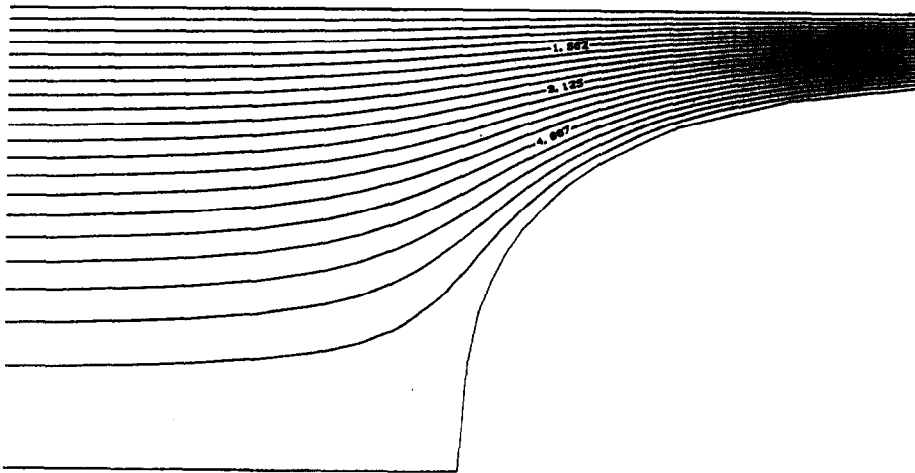

FIG. 7. Streamline map of the flow around a Taylor bubble in stagnant water in a 0.05 m I. D. pipe. The map covers an area of 5 by 2.5 cm, the rise velocity of the bubble is 0.20 m/s, and no surface tension.
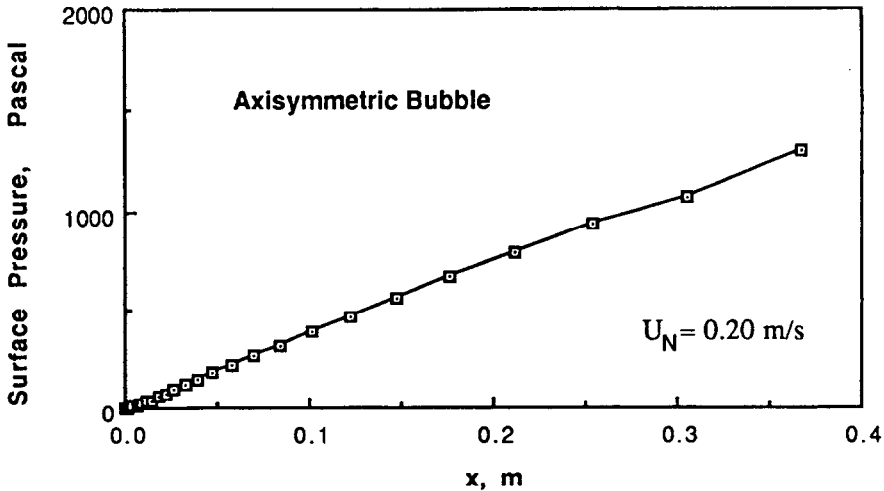
FIG. 8.   Surface pressure profile of a Taylor bubble with specified Dumitrescu shape profile and rise velocity.

in a 0.05 m diameter pipe through stagnant liquid at $U_N = 0.20$ m/s having a shape computed from a solution given by Dumitrescu [2] as shown in Fig. 9 CPU time needed on a HITACHI NAS9000 computer (equivalent to IBM 3033) was approximately 200 s. Computed pressure along the free surface is shown in Fig. 8 and it is evident that the specified shape cannot satisfy the physical requirement of constant pressure along the free surface. Thus, it is necessary to develop a technique to adjust the interfacial shape to meet this constant pressure condition.
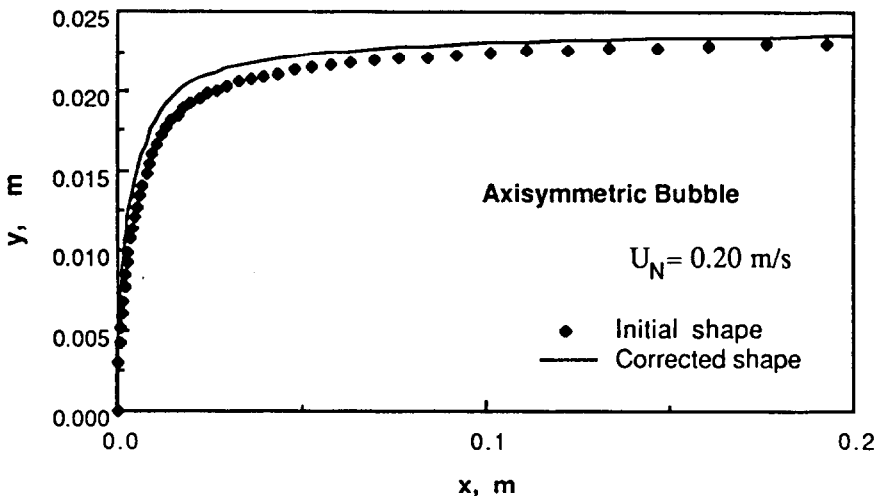

FIG. 9.   The shape profile of a Taylor bubble with designated rise velocity. The solid line indicates the shape profile under constant pressure.

4. Converging on the Shape (Zero Surface Tension)

A method is developed below by which the solution of a first-order differential equation is used in order to converge on the bubble shape profile with constant pressure. We start with the mass conservation and the integral x-direction momentum equations.

$$\rho q \frac{d}{dx}[A\langle uu\rangle] = -\frac{d}{dx}[A\langle p\rangle] + \rho gA + p_{iL}\frac{dA}{dx} - \tau L, \qquad (19)$$

$$A\langle u\rangle = q, \qquad (20)$$

where τ is the wall shear stress, L the wetted perimeter, q the volumetric flow rate in the falling film which is constant over the whole range of x, and $\langle\ \rangle$ indicates an average taken over the flow area. Quantities calculated from the equations after an adjustment in the interface location are designated with a superscript asterisk ($*$). Thus, we have

$$\rho q \frac{d}{dx}[A^*\langle u^*u^*\rangle] = -\frac{d}{dx}[A^*\langle p^*\rangle] + \rho gA^* + p_{iL}^*\frac{dA^*}{dx} - \tau^* L, \qquad (21)$$

$$A^*\langle u^*\rangle = q. \qquad (22)$$

Now, define a velocity shape factor, $\theta(x)$, such that

$$\langle uu\rangle = (1+\theta)\langle u\rangle\langle u\rangle. \qquad (23)$$

Subtracting Eq. (19) from (21) and substituting Eqs. (20) and (22) gives

$$\rho q \frac{d}{dx}\{(1+\theta(x))(\langle u^*\rangle - \langle u\rangle)\}$$

$$= \left[-\frac{d}{dx}(A^*\langle p^*\rangle - A\langle p\rangle) + p_{iL}^*\frac{dA^*}{dx} - p_{iL}\frac{dA}{dx}\right]$$

$$+ [\rho g(A^* - A)] + [-(\tau^* - \tau)L] \qquad (24)$$

or

$$\phi_1 = \phi_2 + \phi_3 + \phi_4, \qquad (25)$$

where ϕ_2 includes all the terms involving pressure in Eq. (24).

Designate $\alpha(x)$ as the ratio of the adjusted to the unadjusted pressure gradient and $\varepsilon(x)$ the fractional change in flow area,

$$\alpha = \frac{dp_{iL}^*}{dx}\left(\frac{dp_{iL}}{dx}\right)^{-1}, \qquad (26)$$

$$\varepsilon(x) = \frac{A^* - A}{A}. \qquad (27)$$

Using

$$\frac{d}{dx}(\langle u^* \rangle - \langle u \rangle) = \frac{d}{dx}\left(\frac{q}{A^*} - \frac{q}{A}\right) = q\left[\frac{\varepsilon}{A^2(1+\varepsilon)}\frac{dA}{dx} - \frac{1}{A(1+\varepsilon)^2}\frac{d\varepsilon}{dx}\right], \quad (28)$$

ϕ_1 can be expressed as

$$\phi_1 = \rho q^2(1+\theta)\left[\frac{\varepsilon}{A^2(1+\varepsilon)}\frac{dA}{dx} - \frac{\varepsilon}{A(1+\varepsilon)^2}\frac{d\varepsilon}{dx}\right] - \frac{\rho q^2\varepsilon}{A(1+\varepsilon)}\frac{d\theta}{dx}. \quad (29)$$

From the definition,

$$\delta p(x) = \langle p \rangle - p_{iL}, \quad (30)$$

ϕ_2 can similarly be expressed in terms of these same quantities in addition to δp^* and δp,

$$\phi_2 = -\frac{d}{dx}\left[(1+\varepsilon)A\delta p^*\right] + \frac{d}{dx}\left[A\delta p\right] + (1-\alpha-\alpha\varepsilon)A\frac{dp_{iL}}{dx}. \quad (31)$$

It is necessary to relate δp^* to ε and other currently known quantities. δp^* is estimated using the y-direction momentum equation in the following manner. In the region of the nose of the bubble the viscous stresses are negligible and this equation can be integrated in the y direction to find $\Delta p(x)$, the difference between the pressure at the wall and the interface,

$$\Delta p = \frac{1}{2}\rho v_i^2 + \int_0^\eta u\frac{\partial v}{\partial x}dy, \quad (32)$$

where v_i is the y-direction velocity at the interface and $\eta(x)$ the shape profile function. From Eqs. (20), (22), and (27), it follows that $\langle u^* \rangle = \langle u \rangle/(1+\varepsilon)$. From the definition of the average velocities and using the fact that for small ε,

$$\frac{1}{1+\varepsilon} \approx 1 - \varepsilon, \quad (33)$$

it can be demonstrated that $u^* = u/(1+\varepsilon)$ as $\varepsilon \to 0$ and the local slope of the streamlines keeps its value, or $(v^*/u^*) \to (v/u)$. Thus $v^* = v/(1+\varepsilon)$ as $\varepsilon \to 0$. Since Δp^* is also defined in Eq. (32), the following relationship is established between Δp^* and Δp,

$$\Delta p^*(x) = \frac{1}{(1+\varepsilon)^2}\Delta p(x).$$

Now it is assumed that in the limit $\varepsilon \to 0$, Δp is proportional to δp; therefore,

$$\delta p^*(x) = \frac{1}{(1+\varepsilon)^2}\delta p(x). \quad (34)$$

Thus, Eq. (31) reads

$$\phi_2 = -\varepsilon A \alpha \frac{dp_{iL}}{dx} + A(1-\alpha) \frac{dp_{iL}}{dx} + A\delta p \frac{d\varepsilon}{dx} + \varepsilon \frac{d}{dx}(A\delta p). \qquad (35)$$

The gravity term in Eq. (24) becomes

$$\phi_3 = \rho g(A^* - A) = \rho g A \varepsilon. \qquad (36)$$

Since the shear stress can be related to the velocity, $\tau \approx (\langle u \rangle - U_N)^n$, the shear stress term can be expressed as

$$\phi_4 = n\varepsilon\tau L \Big/ \left(1 - \frac{U_N A}{q}\right). \qquad (37)$$

In arriving at Eq. (37), the approximation of Eq. (33) is used again. In laminar flow, n is 1. Since the wall stress term is not dominant for a Taylor bubble rising in stagnant liquid, $n = 1$ is used in this study.

The various expressions for ϕ are combined to produce a differential equation for the correction to the shape, $\varepsilon(x)$,

$$a \frac{d\varepsilon}{dx} + b\varepsilon = -(1-\alpha) A \frac{dp_{iL}}{dx}, \qquad (38)$$

where

$$a = \frac{(1+\theta) \rho q^2}{A(1+\varepsilon)^2} + A\delta p,$$

$$b = \frac{d(A\delta p)}{dx} - \alpha A \frac{dp_{iL}}{dx} - \frac{(1+\theta) \rho q^2}{A^2(1+\varepsilon)} \frac{dA}{dx}$$

$$+ \frac{\rho q^2}{A(1+\varepsilon)} \frac{d\theta}{dx} + \rho g A + \frac{\tau L}{1 - U_N A/q}.$$

The computations proceed as follows: Given an initial value of bubble velocity, U_N, and interfacial shape, which fixes $A(x)$, the computational scheme described in Section 3 is carried out until nearly converged. These values of the velocity and pressure fields are used to obtain values of $\theta(x)$, $\delta p(x)$, and τ. Equation (38), the differential equation for $\varepsilon(x)$, is then solved numerically with initial condition $\varepsilon(0) = 0$. Choice of an initial value of α is discussed below. This produces a new profile, $A^*(x)$; then the flow field is computed iteratively, and the solution of the differential equation for $\varepsilon(x)$ and thus for an adjusted $A(x)$ is obtained again. This process is repeated until $\varepsilon(x)$ becomes small. At the same time dp_{iL}/dx becomes

small, i.e., the surface pressure approaches a constant value. In a typical problem, about 500 iterations are necessary to reduce ε to the order of 10^{-5} and this takes 20 min of CPU time on an NAS9000 computer.

A number of precautions are necessary to ensure the overall convergence. Too large a value of ε from the solution of Eq. (38) during the initial iterations will lead to trouble. The initial value of α is arbitrary in the range of 0 to 1. Equation (26) shows that as convergence is approached, α loses physical significance since dp_{iL}/dx and dp_{iL}^*/dx approach zero. It is thus used as a control parameter for ε and its value is arbitrarily selected so that in no case does ε exceeds 0.15. Convergence would proceed more rapidly by using the smallest possible value of α subject to the constraint $\varepsilon \leqslant 0.15$.

Under certain conditions the method of solution outlined here can lead to an artificially wavy interface. The result will be a wave-like behavior of small amplitude having a half-wave length equal to Δx of the cell. This can be easily checked by doubling the grid lines. If waviness once again appears with a characteristic length of the grid dimension, then it is apparent that the waviness is a computational artifact. When this occurs, the final step involves smoothing the surface profile using a quadratic expression for the interface shape over four surface nodes. Computation of the pressure over the smoothed surface made for a series of such runs showed that there was negligible change in meeting the condition of constant pressure at the interface.

The ability of this computational method to arrive at a surface shape which satisfies constant surface pressure conditions is illustrated in Figs. 9 and 10. For the axisymmetric bubble rising at 0.2 m/s the change from the initially assumed shape and the final one is shown in Fig. 9. The pressure along the surface appears in
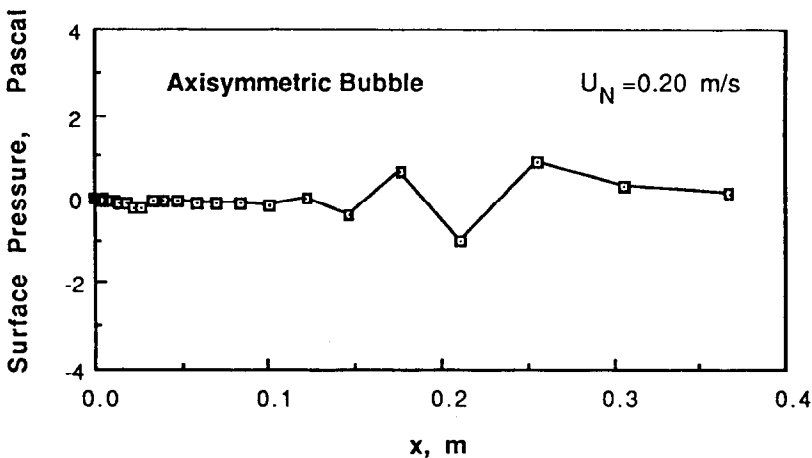

FIG. 10. Surface pressure profile after successful adjustment of the shape profile. The same case is shown in Fig. 8 and 9.

Fig. 10 and should be compared with the results shown in Fig. 8. The variation in pressure across the converged shape is less than 0.2% of the original variation of pressure. Similar computations were carried out for a wide range of bubble velocities and initial shapes for both axisymmetric bubble and for two-dimensional planar bubbles. Figures 11 and 12 show converged shapes for three bubble translation velocities in axisymmetric and planar configurations. Also shown is the interface curvature as a function of position along the surface, s. Note that consistent with the conclusion of Garabedian [10] for potential flow, there exists a converged solution for every bubble velocity. It is now necessary to identify the particular bubble velocity and shape that are physically realistic. Before this is possible, the role of surface tension must be explored.
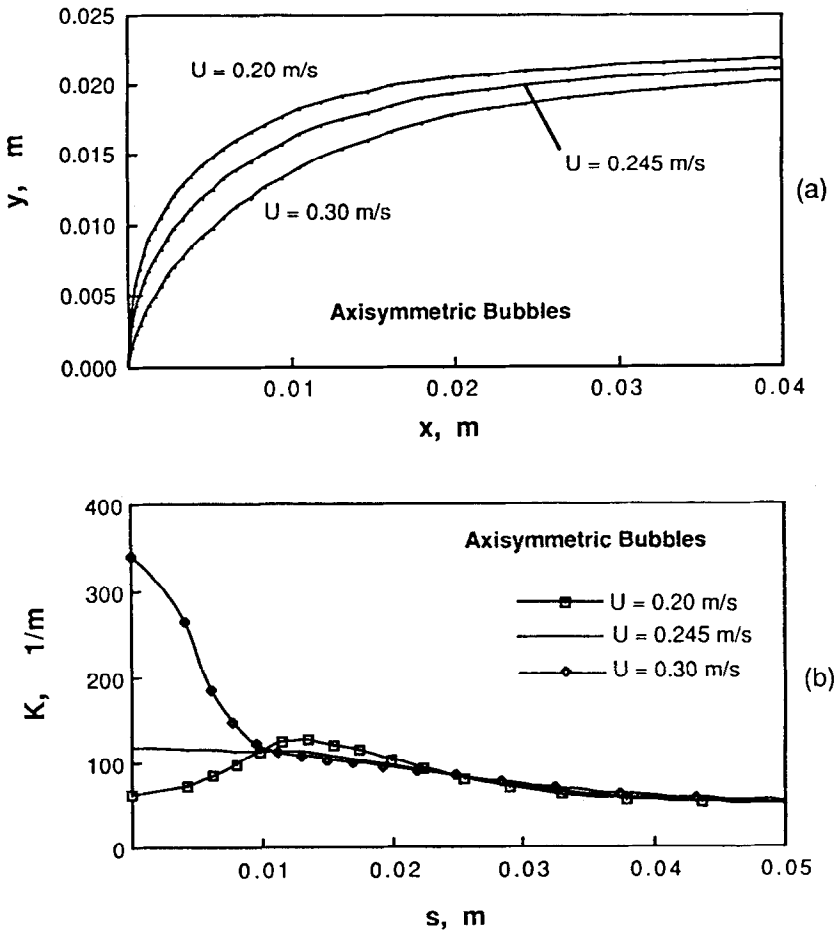

FIG. 11. Axisymmetric Taylor bubbles with designated rise velocity. $D = 0.05$ m, $\mu = 0.001$ N·s/m²: (a) shape profiles; (b) curvature profiles.
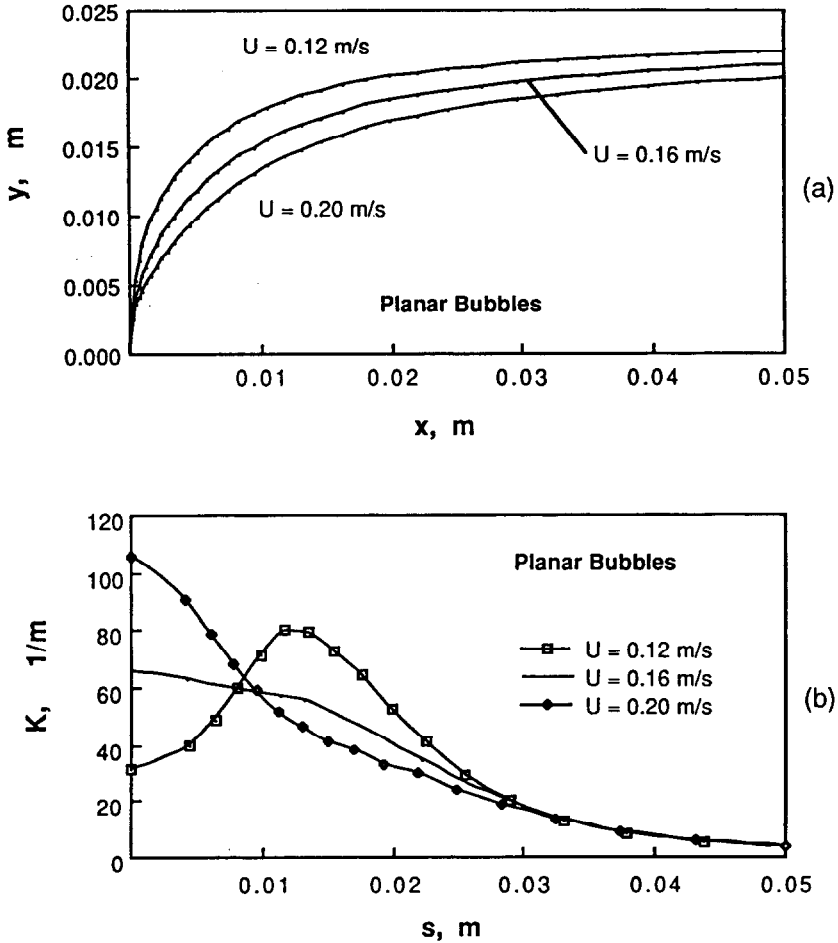
FIG. 12. Planar Taylor bubbles with designated rise velocity, $D = 0.05$ m, $\mu = 0$: (a) shape profiles; (b) curvature profiles.

5. CORRECTING THE SHAPE FOR INTERFACIAL SURFACE TENSION

In the presence of nonzero surface tension the interfacial boundary condition in the liquid is

$$p_{iL} = p_{iG} - p_\sigma, \tag{39}$$

where p_{iG} and p_{iL} are the pressures on the gas and liquid sides of the interface respectively and

$$p_\sigma = \sigma K, \tag{40}$$

where K the curvature is defined by Eq. (7). Clearly K, p_σ, and p_{iL} are functions of x. Thus, the algorithm detailed in Section 4 for finding the interfacial profile by converging on a constant interfacial pressure, p_{iG}, must be modified since in the presence of surface tension, p_{iL} will no longer be constant along the curved surface.

A modified form of Eq. (38) is developed by eliminating p_{iL} using Eq. (39). $\langle p \rangle$ is still obtained by averaging between the wall and p_{iL}; $\delta p(x) = \langle p \rangle - p_{iL} = \langle p \rangle - p_{iG} + p_\sigma$. Substituting the expression of P_{iL} and $\delta p(x)$ into Eq. (24) and reevaluating ϕ_2, Eq. (38) now becomes

$$a_1 \frac{d\varepsilon}{dx} + b_1 \varepsilon = -(1-\alpha) A \frac{dp_{iG}}{dx} - A \frac{d}{dx}(p_\sigma^* - p_\sigma), \qquad (41)$$

where

$$a_1 = \frac{(1+\theta)\rho q^2}{A(1+\varepsilon)^2} + A\delta p,$$

$$b_1 = \frac{d(A\delta p)}{dx} - \alpha A \frac{dp_{iG}}{dx} - \frac{(1+\theta)\rho q^2}{A^2(1+\varepsilon)} \frac{dA}{dx}$$

$$+ \frac{\rho q^2}{A(1+\varepsilon)} \frac{d\theta}{dx} + A \frac{dp_\sigma^*}{dx} + \rho g A + \frac{\tau L}{1 - U_N A/q}.$$

Trial computations show that dp_σ^*/dx changes only a little from iteration to iteration since $\varepsilon(x)$ is usually small. It thus can be estimated using dp_σ/dx in the expression of b_1 where its full value, not the difference, is used.

The last term which appears in Eq. (41) as a result of surface tension introduces

related to the second derivative of A and to ε through Eq. (27). The last term in Eq. (41) thus involves the third derivative of $\varepsilon(x)$. A direct solution of this third-order differential equation in ε is a formidable task as it deals with a boundary value problem requiring a process of shooting at two unknown boundary conditions at the nose. Outlined below is an iterative method which incorporates the important influence of surface tension while working with first-order equations.

Define ε_1 as the solution to Eq. (41) with the surface tension term neglected,

$$a_1 \frac{d\varepsilon_1}{dx} + b_1 \varepsilon_1 = -A(1-\alpha) \frac{dp_{iG}}{dx}. \qquad (42)$$

Set $\varepsilon = \varepsilon_1 - \varepsilon_2$. Then the difference between Eqs. (42) and (41) gives a differential equation for ε_2,

$$a_1 \frac{d\varepsilon_2}{dx} + b_1 \varepsilon_2 = A \frac{d}{dx}(p_\sigma^* - p_\sigma). \qquad (43)$$

Equation (42) can be solved for ε_1 in a manner identical to that described earlier in finding ε with Eq. (38). Initially setting $\varepsilon_2 = 0$, a modified shape can be computed. This and the original shapes are then used to generate $K^*(x)$ and $K(x)$ and values of $(p_\sigma^* - p_\sigma)_1$ and its x derivative as a function of x can be computed. In order to find $(p_\sigma^* - p_\sigma)$ needed for the solution of Eq. (43), a constant γ can be assumed such that

$$d(p_\sigma^* - p_\sigma)/dx = \gamma d(p_\sigma^* - p_\sigma)_1/dx. \tag{44}$$

γ can be shown to be between 0 and -1.0. Note that γ loses its physical significance as convergence is approached and can thus be used as a control parameter for the calculation of ε_2. The substitution of Eq. (44) now makes it possible to solve Eq. (43), a first-order equation for ε_2 using an initial assumption for γ. The new $\varepsilon = \varepsilon_1 - \varepsilon_2$ is then used to adjust the shape of the boundary and the next estimate of $(p_\sigma^* - p_\sigma)$ obtained. The ratio of this new value to $(p_\sigma^* - p_\sigma)_1$, the updated γ, can
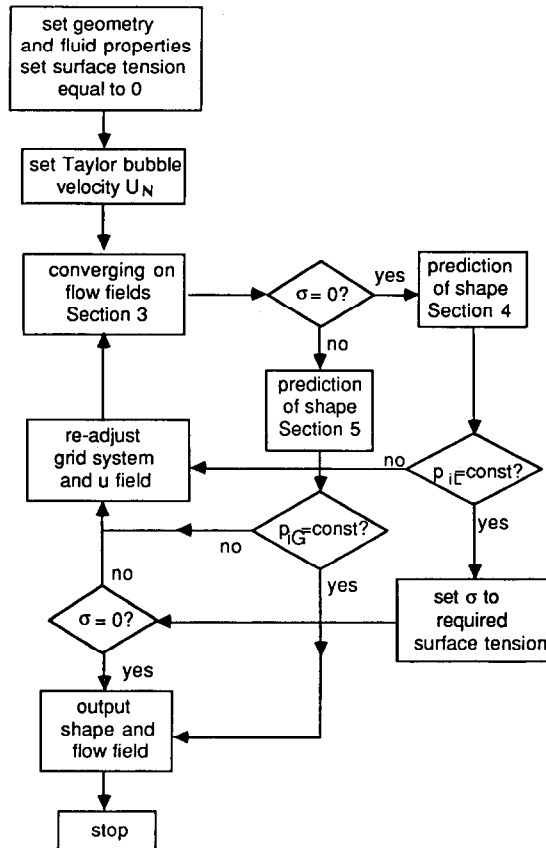

FIG. 13.   Flow sheet of the computational process.

now be compared with the assumed value and a new selection made. It has been found economical of computer time to loop back to the computation of the flow field at this point rather than converge on γ. A convenient initial value for γ has been found to be -0.5; a smaller value approaching zero should be chosen in case that surface tension becomes larger.

The overall computational procedure can be understood by reference to Fig. 13. The algorithm can be viewed in the three parts described in the Sections 3 through 5. This entire process for computing the shape as well as the flow and
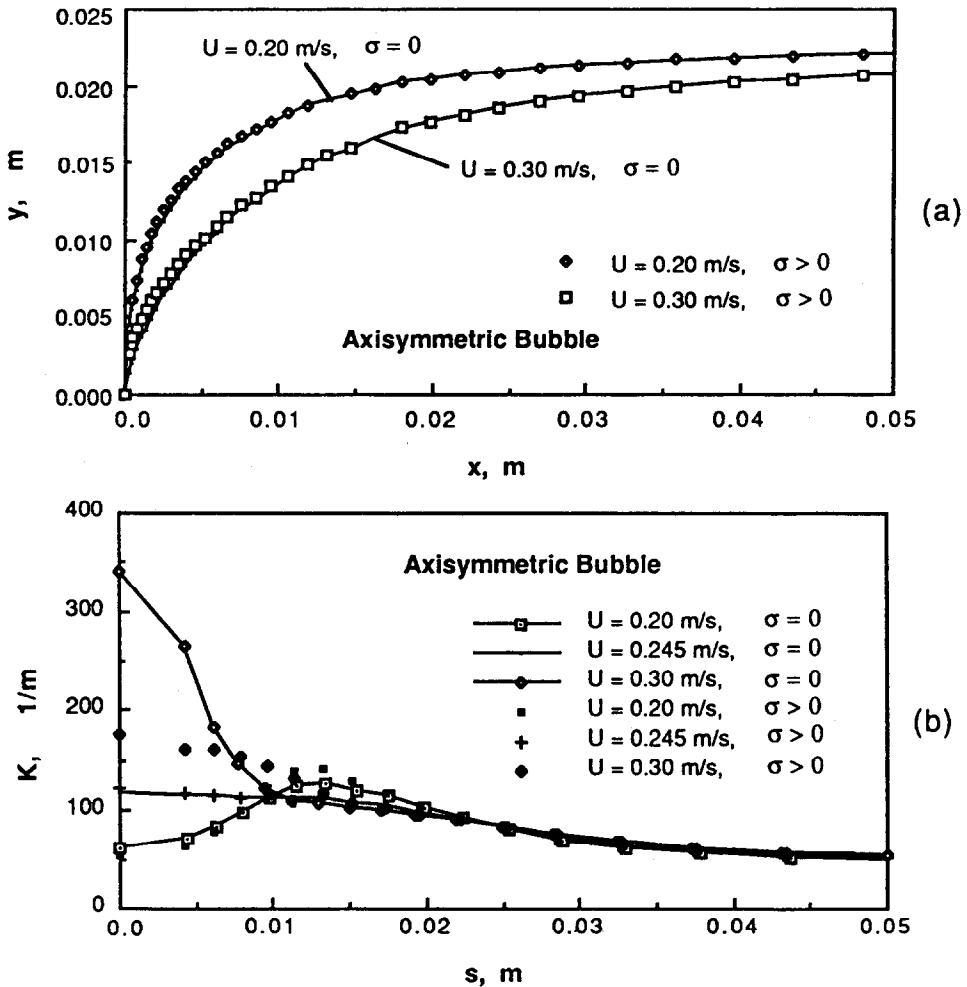

FIG. 14. Effect of the surface tension on the Taylor bubble with designated rise velocity: (a) the shape profiles; (b) the profiles of curvature. The comparison is made between cases with $\sigma = 0$ and 0.075 N/m.

pressure fields for one bubble of specified translation velocity requires about 40 min of CPU time on NAS9000 computer when 52 grid points in the x direction and 39 in the y direction are used.

Figure 14 shows the effect of the surface tension correction on the computed shape for the physical rise velocity for a Taylor bubble in stagnant water (tube I.D. = 5 cm, $\mu = 1$ N.s/m^2 and $\sigma = 0.075$ N/m) The effect appears small on both the shape profile and the curvature near the nose for a bubble rising at a velocity close to the physically observed value (0.245 m/s). But the effect is more significant when the surface tension is larger or the pipe has a smaller diameter. However, as will be shown below, surface tension acts in a subtle manner to isolate that single bubble velocity observed experimentally from the infinite array of possible values all of which satisfy the condition of constant pressure in the gas, no flow across the interface and no shear stress at the interface.

6. A CRITERION FOR SELECTING THE PHYSICALLY OBSERVED VELOCITY OF A TAYLOR BUBBLE FROM THE INFINITY OF POSSIBLE VALUES

Garabedian [10], investigating two-dimensional bubbles rising in an ideal fluid, recognized that multiple solutions exist and suggested that the physically observed rise velocity would be the one which maximizes the rate of dissipation of potential energy as the bubble rises. However, as is apparent from the discussion in Section 4, this maximum increases without bound as the bubbles become more slender and more pointed at the nose. Furthermore, Kelessidis [33] studying Taylor bubbles in an annulus concluded that asymmetric bubbles rise faster than symmetrical ones. But such asymmetry is not observed experimentally in a vertical pipe. In analyzing two-dimensional potential flow around a Taylor bubble, Vanden-Broeck [11, 35] limited acceptable solutions to those whose bubble shape at the nose displayed a zero slope, $d\eta(y)/dy = 0$. This approach placed an upper bound on the translation velocity (critical Froude number $Fr_c = 0.36$, with the definition $Fr = U_N/\sqrt{gD}$), but it still permitted an infinite number of discrete values below this maximum, each of which satisfies the equations of motion and interface boundary conditions with a zero slope at the nose. Couöt and Strumulo [12] also solved for the shape and rise velocity of a two-dimensional Taylor bubble and explained inconsistencies between the work of Vanden-Broeck and Garabedian as due to the number of terms retained in the series expansion for shape. They suggested that the single maximum velocity out of the infinity discrete values would be the one observed in the experiment, although no physical basis for this choice was indicated.

No multiplicity has been reported in the solutions of axisymmetric Taylor bubbles. Earlier investigators [2, 3] assumed the shape of the nose remains spherical over arbitrarily selected lengths of the surface near the nose. By changing that length, the computed value of the translation velocity changes. These solutions do

not satisfy the condition of zero pressure all along the surface. In analyzing the problem where viscous terms are dominant, Reinelt [16] avoided the problem of multiple solutions by arbitrarily specifying the type of the function to depict the bubble shape. By that specification, the shape function was reduced in the vicinity of the nose to $\eta(y) = a + by^2 + cy^4 + \cdots$, since only even powers of y and even Chebyshev polynomials were used. Recently, Bendiksen [6] solved for the potential flow around a Taylor bubble in pipe including the effect of surface tension. He followed the procedures suggested by Dumitrescu [2] to expand a truncated theoretical solution of Stokes stream function ψ into a Taylor series and solved for the coefficients in the ψ expression. By truncating the power series in the equation for the bubble shape $\eta(y)$, he obtained a quadratic equation in $\eta(y)$ and restricted the solutions to two in number, only one of which was physically meaningful. He chose to expand $\eta(y)$ in y^2 and included the surface tension, finally evolving a bubble with a spherical nose.

It is suggested here that in the present of nonzero surface tension, no matter how small the interface must display continuity at the nose. Thus the physically realistic translation velocity results from the action of surface tension on a symmetric bubble, which tends to cause a locally spherical nose. The extent of this sphericity along the surface will vary with magnitude of the surface tension, but in the limit as $x \to 0$, the surface is spherical. The symmetry of the bubble nose requires that the interface be expressed in terms of an even series of y as did Reinelt and Bendickson but we require that the radius of curvature be constant with changes in position along the bubble only at the nose. Thus the criteria is

$$dK/ds = 0, \qquad s \to 0. \tag{45}$$

Now it is possible to extend the computational scheme of Section 6. The gradient dK/ds is evaluated at the nose: if it is positive, the computation is repeated with a larger translation velocity; if negative, a smaller one is used. The converged results are shown in Fig. 15 for an axisymmetric bubble and in Fig. 16 for a two-dimensional bubble ($D = 0.05$ m and $\mu = 0.001$ N·s/m^2). They demonstrate that this criterion, based on an understanding of the role of surface tension, can isolate the physically observed bubble. The solved examples are summarized in Table I. It is noted that no a priori form of shape function is prescribed in this numerical approach. The translation velocity for which $dK/ds = 0$ at $s = 0$ is 0.242 ± 0.002 m/s, yielding a Froude number of 0.345; with $\sigma = 0.075$ N/m, $U_N = 0.241$ m/s or $Fr = 0.344$. Both are in good agreement with the value of 0.35 from the experiments for water. Shown in Fig. 15 are the values of curvature, K, as a function of position along the surface. A simulation for a 2.5 cm diameter tube gave the result of $Fr = 0.344$ for air-water system with $\sigma = 0$, also in excellent agreement. Similar results appear in Fig. 16 for a two-dimensional bubble. Using the same criterion for isolating the physical bubble, the computed translation velocity $U_N = 0.1562$ m/s or $Fr = 0.223 \pm 0.002$ for $\sigma = 0$ and $U_N = 0.1560$ m/s or $Fr = 0.223$ for $\sigma = 0.075$ N/m, while the experimentally accepted value is 0.23.
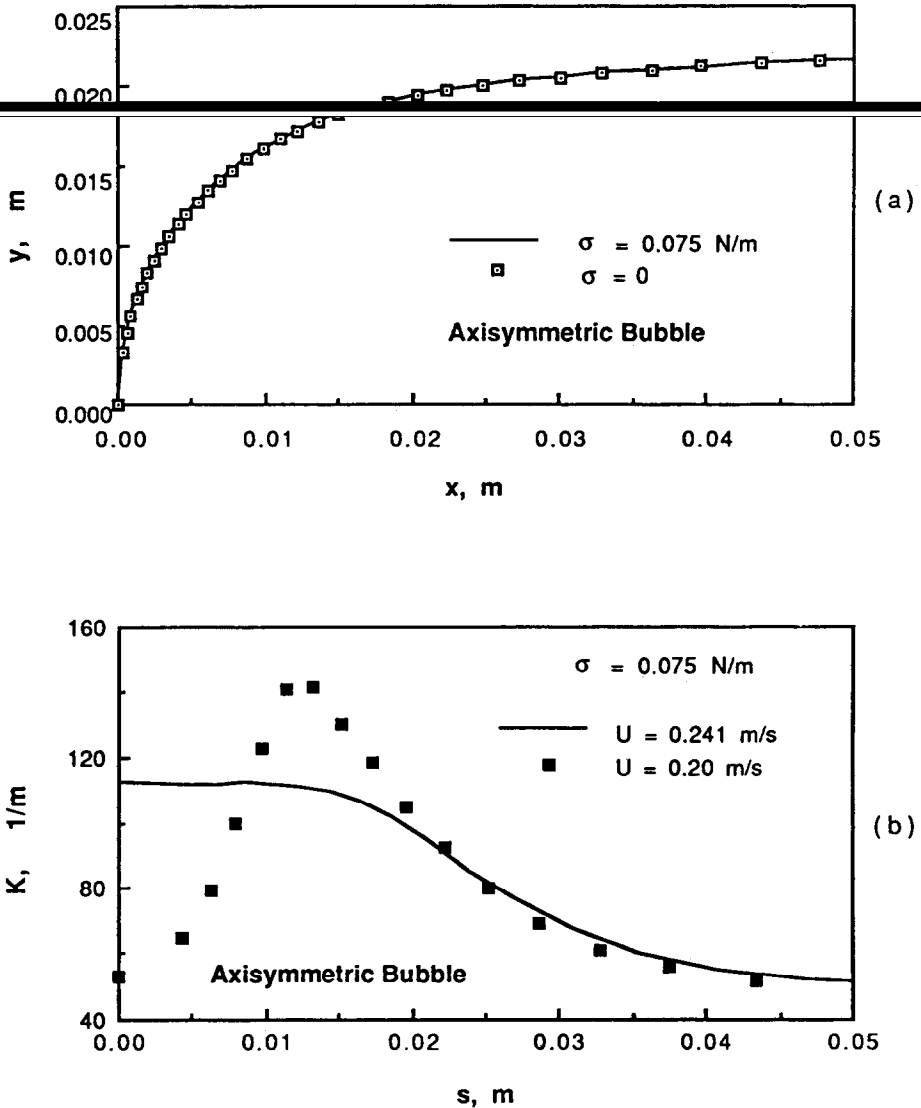
FIG. 15. Computational results of a Taylor bubble with a spherical nose in a 0.05 m I.D. pipe: (a) shape profiles selected by the criterion; (b) curvature profiles for the bubbles with the criterion-selected rise velocity (0.241 m/s) and with specified 0.20 m/s.
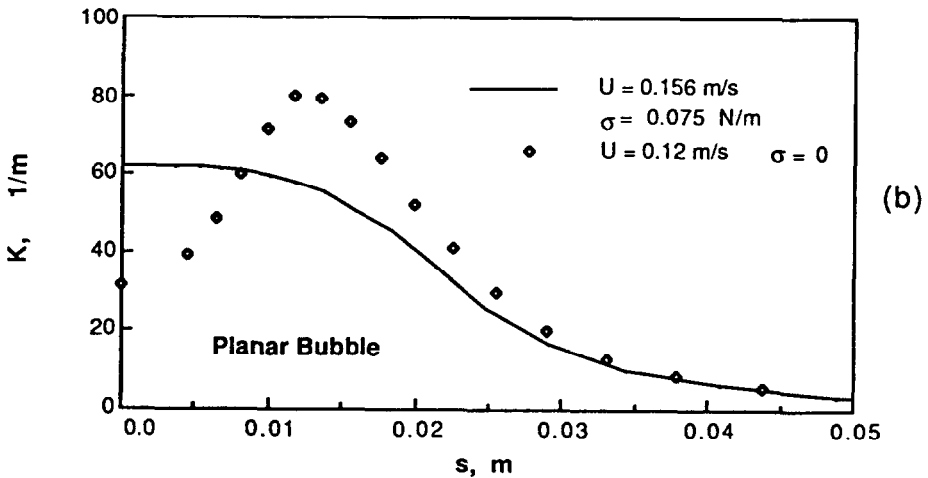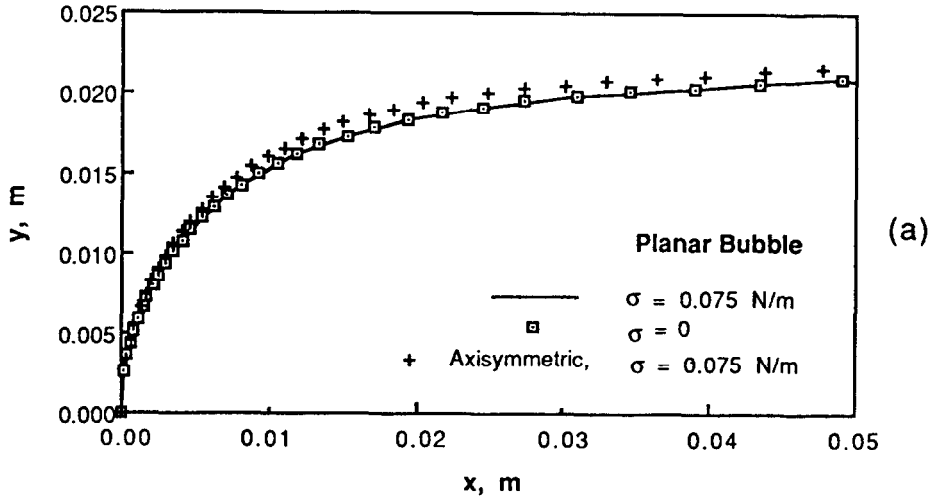
FIG. 16. Computational results of a Taylor bubble with a spherical nose in a $D = 0.05$ m two-dimensional channel: (a) the shape profiles selected by the criterion; (b) the curvature profiles for bubbles with criterion-selected rise velocity ($U = 0.156$ m/s) or the specified $U = 0.12$ m/s. The shape profile of an axisymmetric realistic bubble is shown in (a) for comparison.

TABLE I

Summary of Computational Results

Case	Geometry	D cm	σ N/m	U_N m/s	Fr —	r_N/R —
1	Tube	5	0	0.242	0.345	0.714
2	Tube	5	0.075	0.241	0.344	0.712
3	Tube	2.5	0	0.170	0.344	0.709
4	Channel	5	0	0.1562	0.223	0.653
5	Channel	5	0.075	0.1560	0.223	0.648

Note. $\rho = 1,000 \text{ kg/m}^3$; $\mu = 0.001 \text{ N} \cdot \text{s/m}^2$.

7. SUMMARY AND CONCLUSIONS

A numerical method has been developed for computing the velocity field adjacent to a free surface along with the free surface shape for situations, where both the inertial and viscous terms in the equations of motion can be significant. The method is applied here to the case of a Taylor bubble whose shape is not initially known and which is translating upward in a vertical pipe. A thin liquid film falls around the bubble under the influence of gravity. This simulation is efficient for low viscosity and low surface tension liquids but can be extended for higher viscosity and surface tension.

The methodology incorporates several novel techniques.

(1) The gridding system of Williamson [25] was applied in such a way as to make possible the accurate application of the kinematic and shear stress conditions at the free surface.

(2) A revision to the QUICKER discretizing method is presented which is accurate and converges rapidly for strong upstream convection terms and for conditions, where the velocity vector is highly skewed to the grid.

(3) A method is developed for converging on the shape of the free surface based on the solution of a simple first-order differential equation.

This treatment of the inclined boundary can be extended to a solution domain with two or more monotonic boundary arcs, such as an asymmetric bubble in a plane channel, a solitary wave on a liquid film, etc.

The numerical simulation shows that multiple theoretical solutions exist for both a planar and axisymmetric Taylor bubbles in a pipe. That is, for every possible translation velocity one can find a shape which satisfies the Navier–Stokes equation and the boundary conditions. However, only one such velocity is observed experimentally. A simple geometric criterion has been proposed to single out the physically realistic translation velocity from the infinity of possible values. For any nonzero surface tension, no matter how small, this bubble must have a spherical

nose in the local vicinity of the vertex. As a result the rate of change of curvature there is zero. The simulations show that only at one rise velocity is this criterion satisfied. Predicted values of the rise velocity calculated from such simulations are shown to be in excellent agreement with experiment.

ACKNOWLEDGMENTS

REFERENCES

1. R. D. FERNANDES, R. SEMIAT, AND A. E. DUKLER, *AIChE J.* **29**, 981 (1983).
2. D. T. DUMITRESCU, *Z. Angew. Math. Mech.* **23**, 139 (1943).
3. R. M. DAVIES AND G. TAYLOR, *Proc. Roy. Soc. Ser. A* **200**, 375 (1950).
4. R. COLLINS, *J. Fluid Mech.* **22**, 763 (1965).
5. R. COLLINS, F. F. DE MORAES, J. F. DAVIDSON AND D. HARRISON, *J. Fluid Mech.* **89**, 497 (1978).
6. K. H. BENDIKSEN, *Int. J. Multiphase Flow* **11**, 797 (1985).
7. H. V. NICKENS AND D. W. YANNITELL, *Int. J. Multiphase Flow* **13**, 57 (1987).
8. R. A. S. BROWN, *Canad. J. Chem. Eng.* **43**, 217 (1965).
9. G. BIRKHOFF AND D. CARTER, *J. Math. Mech.* **6**, 769 (1957).
10. P. R. GARABEDIAN, *Proc. Roy. Soc. Ser. A* **241**, 423 (1957).
11. J.-M. VANDEN-BROECK, *Phys. Fluids* **27**, 2604 (1984).
12. B. COUËT AND G. S. STRUMULO, *J. Fluid Mech.* **187**, 1 (1987).
13. F. P. BRETHERTON, *J. Fluid Mech.* **10**, 166 (1961).
14. H. L. GOLDSMITH AND S. G. MASON, *J. Fluid Mech.* **14**, 42 (1962).
15. G. FRIZ, *Zeit. Angew. Phys.* **19**, No. 4, 374 (1965).
16. D. A. REINELT, *J. Fluid Mech.* **175**, 557 (1987).
17. T. Z. HARMATHY, *AIChE. J.* **6**, 281 (1960).
18. E. T. WHITE AND R. H. BEARDMORE, *Chem. Eng. Sci.* **17**, 166 (1962).
19. E. E. ZUKOSKI, *J. Fluid Mech.* **25**, 821 (1966).
20. M. E. WEBER, A. ALARIE, AND M. E. RYAN, *Chem. Eng. Sci.* **41**, 2235 (1986).
21. C. C. MANERI AND N. ZUBER, *J. Fluid Mech.* **1**, 623 (1974).
22. Z.-S. MAO AND A. E. DUKLER, *Chem. Eng. Sci.*, in press.
23. S. B. POPE AND J. H. WHITELAW, *J. Fluid Mech.* **73**, 9 (1976).
24. S. V. PATANKAR, *Numerical Heat Transfer and Fluid Flow* (Hemisphere, Washington, DC, 1980).
25. A. S. WILLIAMSON, *J. Fluid Mech.* **52**, 639 (1972).
26. A. D. GOSMAN AND F. J. K. IDERIAH, TEACH-T: Dept. of Mech. Eng., Imperial College, London, 1976 (unpublished).
27. B. F. ARMALY AND F. DURST, in *Momentum and Heat Transfer Processes in Recirculating Flows*, edited by B. E. Launder and J. A. C. Humphrey (Amer. Soc. Mech. Eng., New York, 1980).
28. B. P. LEONARD, paper presented at the Winter Annual Meeting of ASME, Applied Mechanics Division, New York, Dec. 2–7, 1979.
29. M. A. LESCHNIZER AND W. RODI, *ASME J. Fluid Eng.* **103**, 352 (1981).
30. A. POLLARD AND A. L.-W. SIU, *Appl. Mech. Eng.* **35**, 293 (1982).
31. P. G. HUANG, B. E. LAUNDER, AND M. A. LESCHZINER, *Comput. Methods Appl. Mech. Eng.* **48**, 1 (1985).
32. F. K. WASDEN, Ph.D. dissertation, University of Houston, 1989 (unpublished).
33. S. V. PATANKAR AND D. B. SPALDING, *Int. J. Heat Mass Transfer* **15**, 1787 (1972).
34. V. C. KELESSIDIS, Ph.D. dissertation, University of Houston, 1986 (unpublished).
35. J.-M. VANDEN-BROECK, *Phys. Fluids* **27**, 1090 (1984).